Ann. Geophys. Discuss., https://doi.org/10.5194/angeo-2019-19
Manuscript under review for journal Ann. Geophys.
Discussion started: 14 February 2019

Annales Geophysicae Discussions
Open Access
EGU

Response of low to mid latitude ionosphere to the Geomagnetic storm of September 2017

Nadia Imtiaz[1], Waqar Younas[2], and Majid Khan[2]

[1]Theoretical Physics Division, PINSTECH, Nilore, Islamabad, Pakistan
[2]Quaid-i-Azam University, Islamabad, Pakistan

Correspondence: Nadia Imtiaz (nhussain@ualberta.ca)

Abstract. We study the impact of geomagnetic storm of September 6-9, 2017 on the low-to-mid latitude ionosphere. The prominent feature of this solar event is the sequential occurrence of the two Dst minima of maximum negative values $-148nT$ and $-122nT$ on September 8 at $2UT$ and $15UT$, respectively. The study is based on analyzing the data from GPS stations and the magnetometer observatories located at different longitudinal sectors such as Asia, Africa and America. The GPS data is used to derive the global, regional and vertical total electron content (TEC) in the selected regions. The data of the magnetic observatories is used to illustrate the variation in the magnetic field particularly, the horizontal component of the magnetic field. It is observed that the storm time response of the TEC over the pre-noon sector (Asia) is earlier than Africa and America. The global thermospheric composition maps by Global Ultraviolet Imager exhibits a storm time variation in the O/N_2 ratio. The positive storm effects in the vertical TEC and in the O/N_2 ratio occur in the low latitudes/ equatorial regions.

1 Introduction

It is well known fact that the geomagnetic storm is a temporary variation of the Earth's magnetic field induced by the interplanetary shocks or the high speed solar wind stream (HSSWS). In the modern space era, the strength of the geomagnetic storm is characterized by the minimum Dst (Disturbance- storm time) index and the B_z component of the interplanetary magnetic field (Gonzalez et al. (1994)). On the basis of these parameters the geomagnetic storms can be categorized as: the Small Storm ($Dst \leq -30nT$, $B_z \leq -3nT$), the moderate storms ($Dst \leq -50nT$, $B_z \leq -5nT$), the intense storm ($Dst \leq -100nT$, $B_z \leq -10nT$) and the great storm ($Dst \leq -200nT$) (Tsurutani et al. (1992); Loewe and Prolss (1997)).

The ionosphere features vary along the latitudes and longitudes due to different current systems flowing in the magnetosphere. Therefore, the effects of geomagnetic storms are non uniform in different regions of the magnetosphere. A number of studies have been devoted to investigate the storm effects in different longitudinal and latitudinal sectors. Sharma et al. (2011) investigated the low latitude ionosphere TEC response to the geomagnetic storm of August 25, 2005. On the day of storm, a doubly humped peak in the TEC is observed which is almost two times higher than that of the quiet day value. The first peak is

Ann. Geophys. Discuss., https://doi.org/10.5194/angeo-2019-19
Manuscript under review for journal Ann. Geophys.
Discussion started: 14 February 2019

Annales Geophysicae Discussions

attributed to the prompt penetration effect (PPEF) however, the second peak is due to the plasma fountain effect. It is also found that the prompt penetration effect is almost uniform along the longitudinal direction. Thomas et al. (2016) studied the TEC variations in the mid latitude Northern American sector during the storm time. It is observed that the ionosphere response to the storms is seasonal dependent; i.e., the storms occurring in the summer have large negative effect while the winter events have strong initial positive phase with minimum negative storm effect. Moreover, the events occurring in the fall and spring have almost same effects. Shagimuratov et al. (2012) studied the storm effects in the high latitude regions using the TEC data from International Ground Station network. They found an increase in the TEC at the high latitude polar regions and this disturbance propagates to the mid latitude and equatorial regions. They also investigated that during the southward directed B_z component of the inter planetary magnetic field (IMF), the enhancement in the TEC is stronger than the Northward directed storm period. The author also observed a strong variation in the TEC over the sub-auroral region. Astafyeva et al. (2014) analyzed the effects of super storms having $D_{st} \ll -250nT$ on the ionospheric total electron content. They investigated that depending on the intensity of the storm, the ionospheric TEC may increase from 4 to 40 times of its daily quiet value during the main phase of the storm. The maximum change in the TEC is observed in the auroral oval region.

Jayachandran et al. (2011) have analyzed the GPS-TEC data of the Canadian High Arctic Ionospheric network (CHAIN) to provide clear evidence of a systematic and propagating TEC enhancements produced by the compression of magnetosphere as a result of high solar wind dynamic pressure. By employing the GPS triangulation technique, it is found that the TEC perturbations propagate at a speed of $3-6km/s$ in the anti-sunward direction near the noon sector and $8km/s$ in the sunward direction in the pre-noon low latitude sector. It is also found that these TEC perturbations are associated with the F-region electron density enhancements and with the particle precipitation due to sudden compression of the magnetosphere. Momani has investigated the climatology of the ionospheric TEC at quasi-conjugate points located at different latitudes during the low solar activity in 2007 by using the GPS data. The author has provided a clear evidence of the annual, hemispheric and equinotical asymmetries in the GPS-TEC at all magnetic conjugate stations. There are number of factors that contribute to the observed GPS-TEC asymmetries. For instance, the main causes of the annual asymmetry are: the geomagnetic field topology, the Sun-Earth distance and the lower atmosphere tidal forces. The interhemispheric asymmetry is linked to the solar declination which also leads to the seasonal variations. The equinotical assymetry which is more prominent in the March equinox compared to the September is due to the interhemispheric coupling of the ionosphere Momani (2012). Many authors have analyzed the St. Patrick Day Storm which is the largest geomagnetic storm of the Solar cycle 24 by using different techniques to understand the mechanism of energy transfer and TEC fluctuations. In this context, Nava et al. (2016) investigated the low and middle latitude ionospheric response to the St. Patrick Day Storm of 2015. The storm effects are characterized by using Global and Regional electron content in different longitudinal sectors such as Asia, Africa, America and Pacific. The authors observed a strong enhancement in the American sector. However, the Asian sector shows comparatively large decrease in the vertical TEC. They also used the spectral analysis and magneto-meter data to separate the effects of the convection electric field and of the disturbance Dynamo. Zhang et al. (2018) analyzed this event by using the GPS data of the Crustal movement network of China. It is found that during sudden storm commencement (SSC) phase a rapid enhancement in the ionization distort the

Ann. Geophys. Discuss., https://doi.org/10.5194/angeo-2019-19
Manuscript under review for journal Ann. Geophys.
Discussion started: 14 February 2019

Annales Geophysicae Discussions
Open Access
EGU

Northern equator anamoly. It is also observed that during the main phase a significant decrease in the TEC occurs at the high latitude as compared to the lower latitude region. Watari (2017) presented a study based on the data of about seventeen geomagnetic storms of the solar cycle 24 with minimum $D_{st} \ll -100nT$ which occur during the period $2009 - 2015$ to identify the solar sources of these geomagnetic storms. It is found that the low geomagnetic activity is associated to the weak dawn-to-dusk solar wind electric field. The author has shown that the slow coronal mass ejections play main role in the commencement of geomagnetic storms of the solar cycle 24. Astafyeva et al. (2017) presented a study based on multiple instrument data analysis to investigate the global ionospheric/thermospheric response to the geomagnetic storm of June 22, 2015. Kashcheyev et al. (2018) have made a comprehensive analysis on the basis of two great geomagnetic storms ($Dst \leq -200nT$) which occurred on March 17 and June 22, 2015. It is found that the absence or presence of scintillation in the African sector is associated to the local time at the beginning of the storm. Another finding is that the summer storm results into the formation of plasma bubbles which propagate up to the mid latitude and cause strong scintillation in the GNSS signals. On the basis of this comprehensive analysis, the authors suggested that the factors such as the local time at the commencement of the storm and the season play important role in the modeling of the ionosphere response to the solar activity. Blagoveshchensky and Sergeeva (2019) presented a study based on multi instruments analysis to reveal the variation in the ionospheric parameters during the geomagnetic storm of September 6-10, 2017. Kleimenova et al. (2018) studied the features of the daytime high latitude geomagnetic variations and geomagnetic $pc5$ pulsation during the two stage magnetic storm of September 7-8, 2017. They found that the daytime polar subtorm prohibits the excitation of geomagnetic $pc5$ pulsations over the entire latitude range in which these pulsations were recorded before the daytime bay. This paper aims to investigate the response of low-mid latitude ionosphere to the large geomagnetic storm of September 6-9, 2017. The storm effects are analyzed by using the data from the individual GNSS receivers and the magnetometer observatories located in the three different longitudinal sectors. The approach used in the present study is similar to that used by Nava et al. (2016) and Kashcheyev et al. (2018). The remainder of this article is organized in the following manner: Section 2 deals with the description of data sets and the GPS stations and magnetometers used in our analysis. Section 3 briefly describe the Case study that is the solar event and its characterization on the basis of the global plasma parameters. In Section 4, we present results and a general discussion of our findings. Finally, the conclusions of this study are presented.

2 Data Sets

The following data sets have been used in this study.

1. Solar Event: The NASA's SOHO satellite data provides information about the types of the solar event; e.g., the coronal mass ejection (CME) and the high speed solar wind stream (HSSWS) which are the major sources of the ionospheric perturbations.

Ann. Geophys. Discuss., https://doi.org/10.5194/angeo-2019-19
Manuscript under review for journal Ann. Geophys.
Discussion started: 14 February 2019

Annales Geophysicae Discussions

2. Solar wind parameters: The B_z component of the interplanetary magnetic field (IMF) and the solar wind speed (V_{sw}) are provided by the ACE satellite.

3. Geomagnetic indices: The world data center for Geomagnetism, Kyoto provides information about different geomagnetic storm indices that is AE and $SYM-H$. The magnetic Index $SYM-H$ measures the magnetosphere electric currents known as the ring currents which decreases the Earth's magnetic field. The auroral electrojet (AE) index estimates the energy transferred from storm to the Auroral ionospheric regions.

4. Electron Content Data: The Global Ionospheric Maps (GIMs) have been used to perform the analysis of the Total electron content variations during the storm period under consideration. The Global Electron content is the total number of electrons present in the ionosphere at fixed altitude of about $450Km$. The GEC is calculated by using Afraimovich et al. (2006) approach; i.e., multiplying each GIM cell by its corresponding vTEC value and is given by,

$$GEC = \sum_{i,j} I_{il} S_{ij},$$

where i and j represent the latitude and longitude of each GIM cell respectively. S_{ij} is the area of each GIM cell, I is the corresponding vTEC value and summation is taken over the entire GIMs maps. The Regional electron Content (REC) is the total number of electrons in the specified region of the ionosphere. Our analysis based on the three different regions: Asia ($60° : 150°E$), Africa ($-30° : 60°E$), America ($-120° : -30°E$). The REC is calculated similar to that of the GEC with the summation is restricted to the GIM cells of that particular region only.

5. GPS stations: The data of nine GPS stations is analyzed. These stations are selected on the basis of data availability and their geographic location. The geographic coordinates of these stations are given in Table 1.

6. Magnetometer Data: The storm time magnetic field variations are analyzed by using the data from three low latitude observatories in three sectors: Asia (KOU), Africa (MBO) and America (GUA). The quasi-definite data of these observatories which is available at inter-magnet.com have been used for the analysis. Table 2 shows the geographic location of these observatories.

7. Thermospheric Composition: For the analysis of the storm time variation in the thermospheric neutral composition, the global maps of O/N_2 obtained from the GUVI/TIMED are presented here.

3 Case Study

We are considering the space weather event occurred during September 6-12, 2017. A Coronal Mass Ejection (CME) originating from the $X9.3$ solar flares on September 6, 2017, reached on the Earth at $23:04UT$ on September 7, 2017. After the arrival of the CME, a strong geomagnetic storm G_3 has been triggered at $23:25UT$. The impact of the CMEs further lead to a

Ann. Geophys. Discuss., https://doi.org/10.5194/angeo-2019-19
Manuscript under review for journal Ann. Geophys.
Discussion started: 14 February 2019

Annales Geophysicae Discussions

severe geomagnetic storm G_4 with the value of geomagnetic index $k_p = 8$ at $23:50UT$. The global morphology of this solar event is illustrated in Figure 1. The solar wind speed increased from 500 to $785km/s$. The geomagnetic Index Kp reached 8. The B_z component of the interplanetary magnetic field shows rapid variation during the storm period. After the shock arrival, the B_z component decreases reaching to the value $-30nT$ and then it rapidly increases to the value of approximately $+15nT$. It again performs a negative excursion and reaches to the value of approximately $-20nT$. It can be seen that the $SYM-H$ index also follows the behavior of the B_z component. When the B_z becomes negative, the $SYM-H$ also decreases to the its negative value of $\leq -150nT$ and therefore, produces the first minima of the $SYM-H$ index at $2UT$. Now as the B_z increases to the positive value, the $SYM-H$ also becomes less negative reaching to the value of $-50nT$ and then with the negative excursion of the B_z it decreases again to the second minimum value of $\leq -130nT$ at $15UT$. Therefore, the two pronounced minima of the $SYM-H$ index with values $-148nT$ and $-122nT$ at $2UT$ and $15UT$ respectively are observed on September 8, 2017. It can be noticed that the intensity of the first minimum of $SYM-H$ is higher than that of the second minimum. The auroral activity also increases and the two peaks in the AE index having values of $2000nT$ and $2500nT$ coinciding with the two minima of the $SYM-H$ index are also observed.

4 Results/Discussion

In this section, we present the variation of the diverse parameters such as the Regional Electron content (REC), the Global Electron Content (GEC), the vertical Electron Content (vTEC), the magnetic field and the O/N_2 ratio as a result of the geomagnetic storm of September 6-9, 2017. Figure 2 shows difference of the Regional Electron Content (REC) (top), the Global Electron Content (GEC) (middle) and the Dst Index (bottom) during the period September 6-12, 2017. The difference in the GEC and REC is calculated by using the five quiet days before the storm. It can be seen that the GEC shows two positive peaks at $2UT$ and $15UT$ corresponding to the first and second minima of the Dst index. In order to find the region which causes the peak in the GEC, the REC is plotted for the three longitudinal sectors: Asia ($60°E$:$150°E$) , Africa ($-30°E:60°E$), America ($-120°E:-30°E$). The REC plot shows that the first peak in the GEC is due to the Asian sector however, the second peak is due to the African and American sectors.

The nine panels of Figure 3 illustrate the variation of the vTEC for the individual station of the three longitudinal sectors from September 2-18, 2017. In Figure 3, the panels first to third represent the stations of the Asian sector; i.e., BJFS, BAKO and YAR2, the panels four to six represent the African sector; i.e., NOTI, NKLG and WIND. The panels seven to nine represent the stations of the American sector; i.e., BOGT, AREQ and ANTC. On each panel the vTEC is plotted in red with daily quiet variations in blue which is calculated by using five quiet days before the storm. The following pertinent features of the vTEC can be noticed:

- On the day of the storm, the Northern and Southern mid latitude stations in the Asian sector show slight increase in the vTEC. On the day after the storm, the vTEC decreases for these two stations. A double peak structure of the vTEC is also noticed for the Southern mid latitude station YAR2.

Ann. Geophys. Discuss., https://doi.org/10.5194/angeo-2019-19
Manuscript under review for journal Ann. Geophys.
Discussion started: 14 February 2019

Annales Geophysicae Discussions

Table 1. Locations of the GPS stations used in the analysis.

Station	Sector	Geographic Latitude	Geographic Longitude
BJFS	Asia	$39.60^{\circ}N$	$115.89^{\circ}E$
BAKO	Asia	$6.49^{\circ}S$	$106.85^{\circ}E$
YAR2	Asia	$29.04^{\circ}S$	$115.35^{\circ}E$
NOTI	Africa	$36.87^{\circ}N$	$14.98^{\circ}E$
NKLG	Africa	$0.35^{\circ}N$	$09.67^{\circ}E$
WIND	Africa	$22.57^{\circ}S$	$17.09^{\circ}E$
AREQ	America	$16.50^{\circ}S$	$71.50^{\circ}W$
BOGT	America	$4.64^{\circ}N$	$74.08^{\circ}W$
ANTC	America	$37.34^{\circ}S$	$71.53^{\circ}W$

– In the African region, the largest increase in the vTEC is observed for the equatorial latitude station NKLG during the storm. However, the increment is less significant in the other stations. On day after the storm, a negative storm is observed in the Northern mid-latitude station.

– In the American sector, the three stations show similar behavior that is the vTEC increases on the day of the storm. The largest increase in the vTEC is observed for the equatorial station BOGT during the storm period. It can also be noticed that the vTEC decreases significantly for this station after the day of storm. Both the Southern mid latitude and equatorial trough stations ANTC and AREQ depict a multi-peak structure of the vTEC on the day of storm. However, on the day after the storm the ionization disappears at the southern mid latitudes and the vTEC returns to its quiet value.

Figure 4 illustrates the variation of vTEC as a function of time and latitude over the three longitudinal sectors that is Asia (first panel), Africa (second panel) and America (third panel). These TEC maps cover the period from September 4-12, 2018. The Dst index over this period is also shown at the bottom in Figure 4. The vTEC maps of the three longitudinal sectors show following features:

– In the Asian sector, a regular pattern of the vTEC is observed except on the day of the storm. However, both the African and American sectors show irregular pattern of the vTEC.

– In the Asian sector, the largest increase in the vTEC is observed on early September 8. However, the American sector shows the largest increase in the vTEC on the September 8.

– Most of the total electron content is confined to the lower latitudes and to the equatorial regions.

– After the storm, the ionization or TEC reduces significantly and returns to its quiet value.

The three plots in Figure 5 represent the magnetometer variations monitored at the three equatorial magnetic observatories corresponding to the three longitudinal sectors Asian (GUA), Africa (MBO) and America (KOU). Each plot shows variation

Ann. Geophys. Discuss., https://doi.org/10.5194/angeo-2019-19
Manuscript under review for journal Ann. Geophys.
Discussion started: 14 February 2019

Annales Geophysicae Discussions

Table 2. Locations of the Magnetometers used in the analysis.

Station	Sector	Geographic Latitude	Geographic Longitude
GUA	Asia	$13.59^{\circ}N$	$144.87^{\circ}E$
MBO	Africa	$13.34^{\circ}N$	$16.97^{\circ}W$
KOU	America	$5.21^{\circ}N$	$52.93^{\circ}W$

in the H component of the magnetic field (in black), the daily quiet variation (S_q) (in blue) and the disturbances (D_l^h) (in red). The following common behavior of the H component is noticed in the three sectors:

- During the initial phase of the storm on September 7, 2017, the Chapman-Ferraro current associated with the contraction of the magnetosphere due to high solar wind pressure leads to the enhancement of the H component.
- During the main phase of the storm on September 8, 2017, the enhanced ring current in the magnetosphere strongly reduces the H component.
- Following the strongest decrease in the H component, the ring current decays and the recovery phase started which lasted for several hours.
- During the recovery of the first storm, a relatively less decrease in the H component due to the commencement of the second storm is noticed on late September 8.
- The largest disturbance of the H component of magnetic field with amplitude $-180nT$ is observed at MBO as compared to $-150nT$ at KOU and $-140nT$ at GUA.

Another effect that can bee seen during the storm is the variation in the the thermospheric neutral composition. The storm strengthens the vertical and meridional winds which lead to the variation in the thermospheric neutral profile. The global view of the thermospheric O/N_2 ratio obtained from the TIMED/GUVI for the period September 7-10, 2017 is shown in Figure 6. On the day of the storm, a significant enhancement in the O/N_2 ratio is observed at the low and equatorial latitudes. This observation is consistent with the behavior of the vTEC during the storm period. After the recovery of the storm, the thermospheric composition return to its normal profile.

5 Conclusions

We presented the impact of geomagnetic storm of September 6-10, 2017 on low-mid latitude ionosphere over the three longitudinal sectors; i.e., Asia, Africa and America. The storm effects are characterized by using diverse parameters including the global, regional and vertical total electron content derived from the GPS data, the horizontal component of the magnetic field obtained from the magnetometers and the neutral composition from the GUVI/TIMED. It is observed that moderately positive storm effects occur in all longitudinal stations. However, the temporal response of the three sectors shows that the positive

Ann. Geophys. Discuss., https://doi.org/10.5194/angeo-2019-19
Manuscript under review for journal Ann. Geophys.
Discussion started: 14 February 2019

storm effect in the REC and vTEC over the Asian sector is observed earlier than the American sector. Most of the TEC is confined to the equatorial and low latitude regions. The storm time enhancement in the neutrals ratio; i.e., O/N_2 over the low latitudes and equator is consistent with the observed TEC behavior. However, the negative storm effect in the O/N_2 ratio can be observed in the higher and mid latitude regions. The study would be useful for the understanding of storm time response of the low-mid latitude ionosphere.

Acknowledgements. he authors are grateful to the space weather data resource https://omni-web.gsfc.nasa.gov/ for providing the solar wind data, to the World Data Center for Geomagnetism at Kyoto University, Japan for providing the geomagnetic data, to the International GNSS Service (IGS) team for providing the GPS data and to the https://ssusi.jhuapl.edu/. The data analysis techniques have been learned during the hands on session in the Workshop Space Weather impact on the low latitude GNSS operation at ICTP. NI acknowledge the UNOOSA/ICTP for providing the financial support to attend this workshop and learn these techniques. This research work was partly supported by the HEC Pakistan: $GrantNo.7632/Federal/NRPU/RD/HEC/2017$.

Ann. Geophys. Discuss., https://doi.org/10.5194/angeo-2019-19
Manuscript under review for journal Ann. Geophys.
Discussion started: 14 February 2019

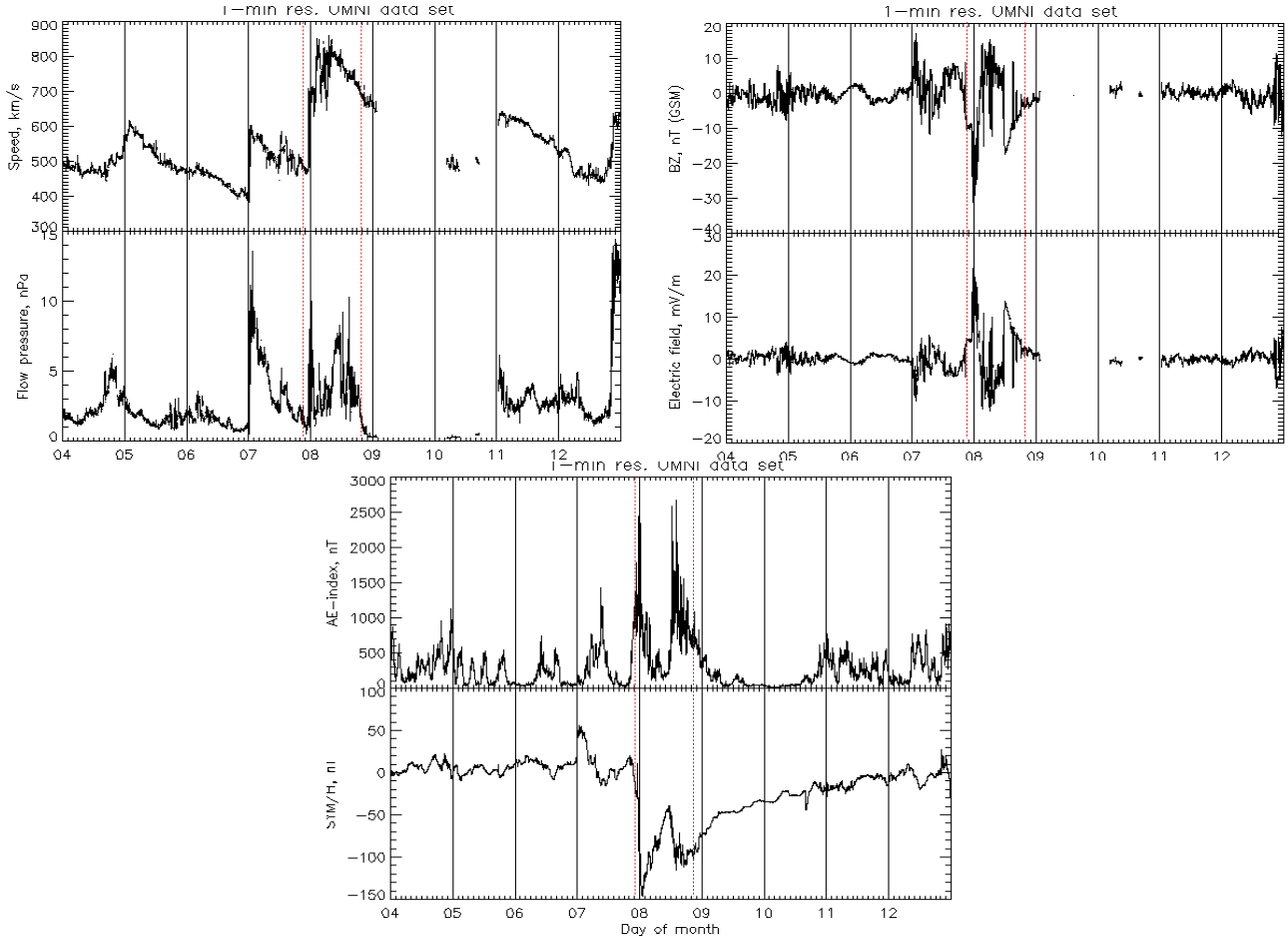

Figure 1. Global parameters: the solar wind speed, the flow pressure, the B_z component, the Electric field, the Auroral index and the $SYM-H$ index characterizing the geomagnetic storm during the period of September 4-12, 2017

References

Astafyeva, E., Yasyukevich, Y., Maksikov, A., Zhivetiev, I., 2014, Space Weather, 12.

Astafyeva, E., Zakharenkova, I., Huba, J. D., Doonbas, E., and Van den IJssel, J., 2017, J. Geophys. Space Sci., 122.

Afraimovich, E. L., E. I. Astafyeva, and I. V. Zhivetiev (2006), Earth Sci.,409A(N6), 921–924.

Blagoveshchenskya, D. V. and Sergeeva, M. A. 2019, Advances in Space Research, 63.

Gonzalez, W.D., Joselyn, J. A., Kamide, Y., Kroehl, H. W., Rostoker, G., Tsurutani, B. T., and Vasyliunas, V. M. (1994), J. Geophys. Res., 99 (A4), 5771-5792.

Jayachandran, P. T., Watson, C., Rae, I. J., MacDougall, J. W., Chadwick, R., Kelly, T. D., Prikryl, P., Meziane, K. and Danskin, D. W., Shiokawa, K. 2011, J. Geophys. Res., 38.

Ann. Geophys. Discuss., https://doi.org/10.5194/angeo-2019-19
Manuscript under review for journal Ann. Geophys.
Discussion started: 14 February 2019

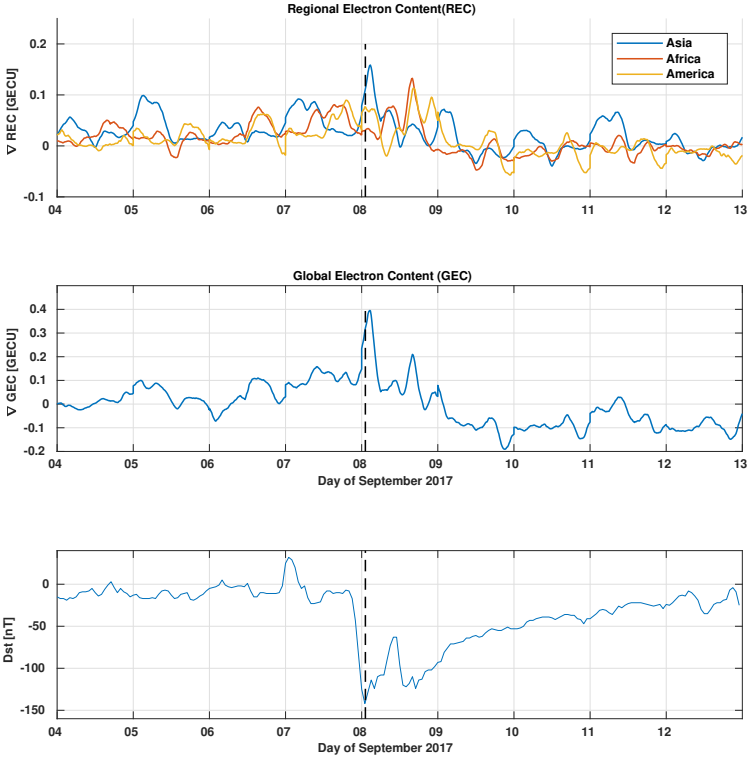

Figure 2. Variation of the Regional electron content (top), the Global electron content (middle) and the Dst index (bottom) during the geomagnetic storm of September 6-9, 2017

Kashcheyev, A., Migoya-Orué, Y., Amory-Mazaudier, C., Fleury, R., Nava, B., Alazo-Cuartas, K., and Radicella S.M. 2018, J. Geophys. Res., 123.

Kleimenova, N. G., Gromova, L. I., and Malysheva, L. M., 2018, Geomagnetism and Aeronomy, 58, 597-606.

Loewe, C. A., and Prolss, G. W. (1997), J. Geophys. Res., 102, 209–213.

Momani, M. A. 2012, Radio Science, 47.

Nava, B., Zuluaga, J. R., Alazo-Cuartas, K., Kashcheyev, A., Migoya-Orué, Y., Radicella S. M., Mazaudier, C. A. and Fleury, R. 2016, J. Geophys. Res., 21.

Shagimuratov, I. I., Krankowski, A., Ephishov, I., Cherniak, Y., Wielgosz, P. and Zakharenkova, I. (2012), Advances in Sp. Res., 6.

Sharma, S., Galav, P., Dashora, N., Alex, S., Dabas, R.S., Pandey, R. 2011, J. Geophys. Res., 116.

Thomas, E.G., Baker, J. B. H., Ruohoniemi, J. M., Coster, A. J., Zhang, S. -R. 2016, J. Geophys. Res., 121.

Tsurutani, B. T., Lee, Y. T., Gonzalez, W. D., and Tang, F. (1992), Geophys. Res. Lett., 19, 73–76, doi: 10.1029/91GL02783.

Watari, S. 2017, Earth, Planets and Space, 69.

Zhang, W., Zhao, X., Jin, S. and Li, J. 2018, Geodesy and Geodynamics, 9.

Ann. Geophys. Discuss., https://doi.org/10.5194/angeo-2019-19
Manuscript under review for journal Ann. Geophys.
Discussion started: 14 February 2019

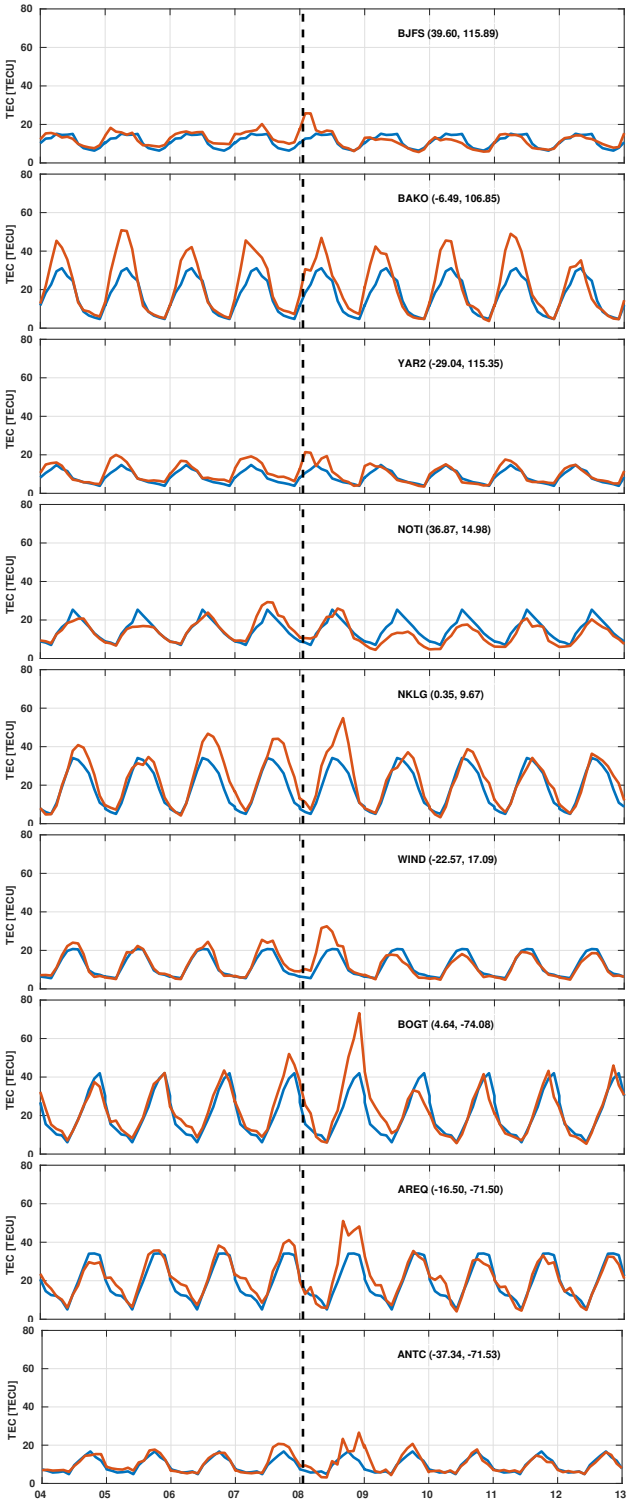

Figure 3. The vTEC variations at GPS stations during the geomagnetic storm of September, 2017. Each panel illustrates the disturbed vTEC (in orange) and its quiet value (in blue)

Ann. Geophys. Discuss., https://doi.org/10.5194/angeo-2019-19
Manuscript under review for journal Ann. Geophys.
Discussion started: 14 February 2019

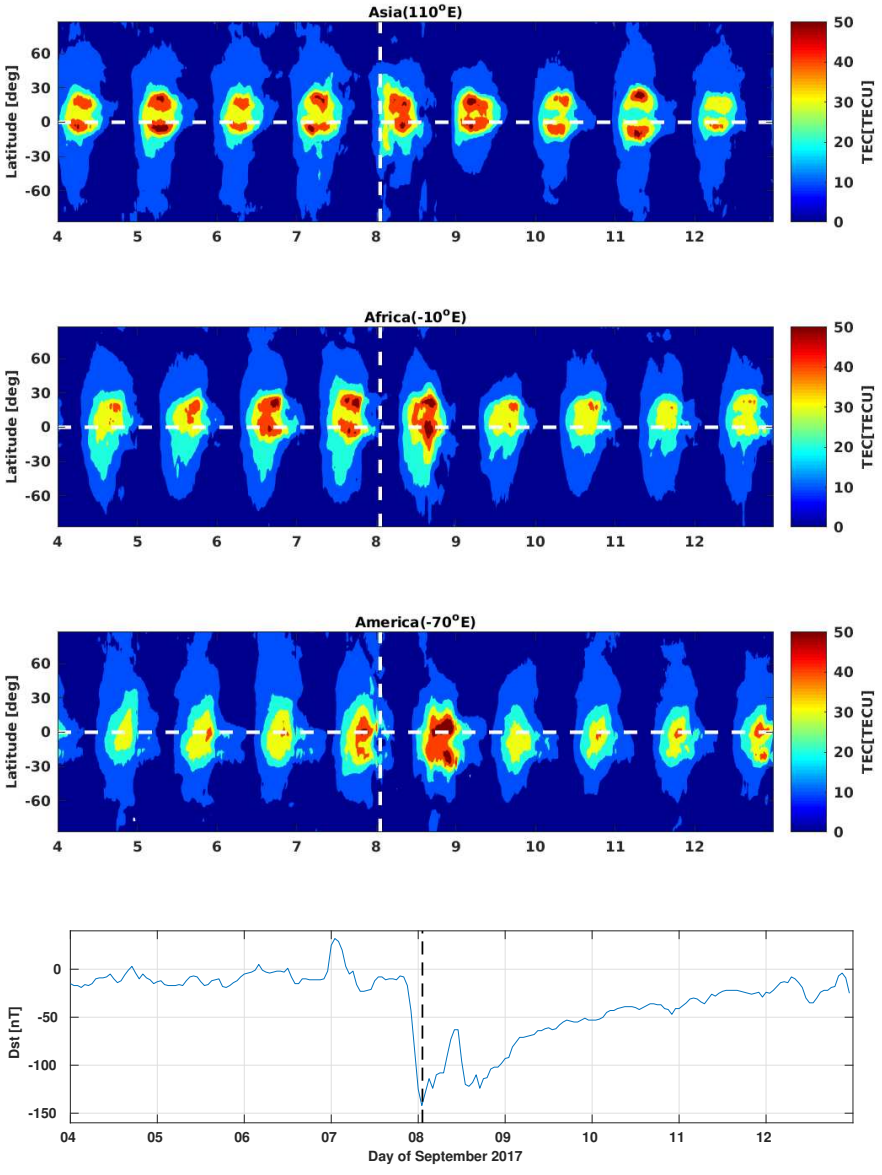

Figure 4. The vTEC variations over the Asian (first panel), African (second panel), American (third panel) sectors and the Dst index (fourth panel) during the geomagnetic storm of September 6-9, 2017

Ann. Geophys. Discuss., https://doi.org/10.5194/angeo-2019-19
Manuscript under review for journal Ann. Geophys.
Discussion started: 14 February 2019

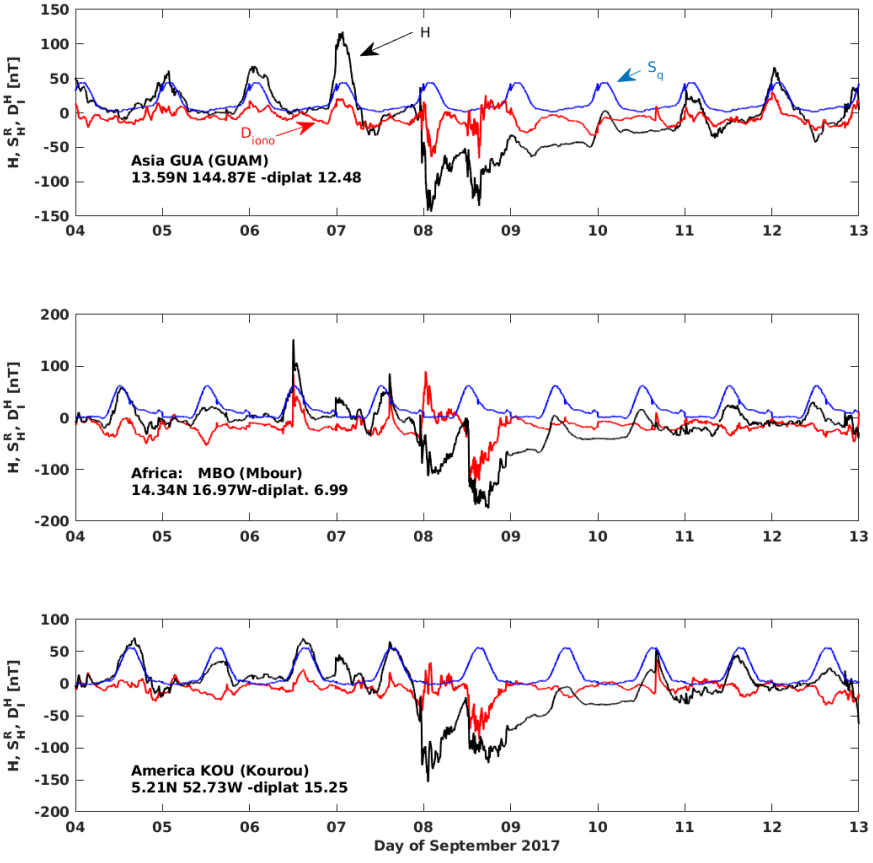

Figure 5. The magnetometer H variations at specific stations during September 4-12, 2017 over the three sectors: the Asian (top), the African (middle) and the American (bottom). On each panel the daily quiet variations (blue), the actual H variations (black) and the ionosphere disturbance current (blue) are plotted

Ann. Geophys. Discuss., https://doi.org/10.5194/angeo-2019-19
Manuscript under review for journal Ann. Geophys.
Discussion started: 14 February 2019

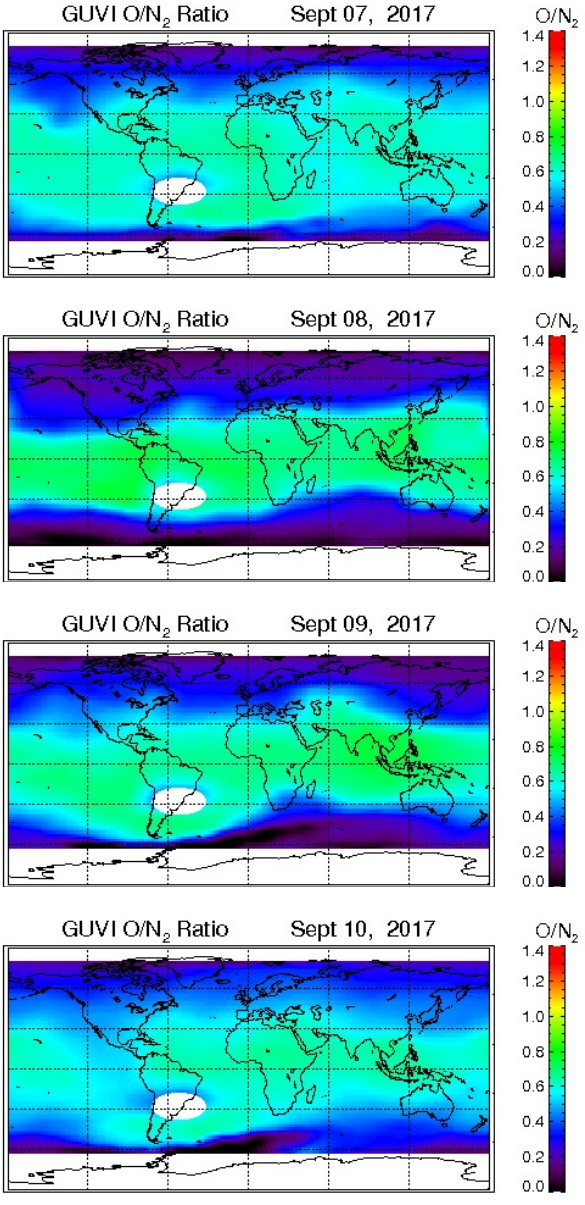

Figure 6. The thermospheric O/N_2 ratio obtained from the GUVI/TIMED during September 7-10, 2017